

On the Performance of the Savonius Wind Turbine

V. J. Modi

Professor,
Fellow, ASME

M. S. U. K. Fernando

Postdoctoral Fellow.

Department of Mechanical Engineering,
The University of British Columbia,
Vancouver, B. C., Canada V6T 1W5

An extensive wind tunnel test program is described which assesses the relative influence of system parameters on the Savonius rotor performance. The parametric study leads to an optimum configuration with an increase in efficiency by around 100 percent compared to the reported efficiency of ≈ 12 -15 percent. Of particular interest is the blockage correction procedure which is vital for application of the wind tunnel results to a prototype design, and facilitates comparison of data obtained by other investigators. Next, using the concept of a central vortex, substantiated by a flow visualization study, a semiempirical approach to predict the rotor performance using measured stationary blade pressure data is developed. The simple approach promises to be quite effective in predicting the rotor performance, even in the presence of blockage, and should prove useful at least in the preliminary design stages.

Introduction

The Savonius rotor concept never became popular, until recently, probably because of its low efficiency. However, it has the following advantages over the other conventional wind turbines:

- simple and cheap construction;
- acceptance of wind from any direction thus eliminating the need for reorientation;
- high starting torque;
- relatively low operating speed (rpm).

The above advantages may outweigh its low efficiency and make it an ideal economical source to meet small scale power requirements, especially in the rural parts of developing countries. It has also been proposed as an auxiliary starting device for the Darrieus turbine [1], and as a tidal power generator [2]. The concept of the Savonius rotor was based on the principle developed by Flettner. Savonius used a rotor which was formed by cutting the Flettner cylinder into two halves along the central plane and then moving the two semicylindrical surfaces sideways along the cutting plane so that the cross-section resembled the letter "S." An "optimum" geometry was obtained by systematically testing more than 30 different models in a wind tunnel, and Savonius reported encouraging results. He conducted further tests in natural wind and observed that the rotor ran at a higher speed than that in the wind tunnel for the same wind velocity. According to Savonius the best of his rotors had a maximum efficiency of 31 percent, while the maximum efficiency of the prototype was 37 percent [3]. However, other researchers who have conducted similar experiments with the Savonius rotor have not agreed with the claimed efficiencies [4-5].

Following Savonius, Bach, Newman, Sivasegaram, Khan, and Blackwell et al. [5-10], among others, conducted several experiments to investigate the effect of geometrical parameters

such as blade gap size, overlap etc., the effect of Reynolds number and the use of augmentors. Jones et al. conducted some flow visualization studies to help understand the associated flow behavior [2].

Based on a careful evaluation of the experimental procedures, measuring techniques, and the available data, the following general remarks can be made:

(a) As can be expected, earlier tests did not have the advantage of reliable and sophisticated instrumentation.

(b) Almost all the tests were carried out using models in fairly small wind tunnels. As a result the corrections due to blockage were substantial, and, hence, the accuracy of the measurements suffered.

(c) In a number of cases blockage corrections were completely ignored. When applied, the procedure was mostly empirical and unreliable.

(d) In all the test results, bearing friction losses were neglected. Unfortunately, due to small models, they may affect the performance substantially.

The present work describes the development of a Savonius rotor configuration, simple in design, fabrication, and maintenance, yet having a reasonably high efficiency. It is suitable for rural small scale applications in developing countries.

The experimental methodology and the corresponding results of the systematic optimization process undertaken, to develop an efficient Savonius rotor configuration, are presented. Special care has been taken to overcome the problems which led to unreliable results found in the literature. Focus is on the two-bladed configuration with geometric parameters varied in an extensive wind tunnel test program. Effect of the blade geometry, wind tunnel blockage as well as frictional losses in the model mounting bearings are assessed. The pressure distribution and starting torques have been measured for the stationary blade at different angles.

A semiempirical approach using the quasi-steady method, similar to the blade element theory, with a central vortex at the core, and the measured pressure data as an input is described.

Contributed by the Solar Energy Division of the AMERICAN SOCIETY OF MECHANICAL ENGINEERS for publication in the JOURNAL OF SOLAR ENERGY ENGINEERING. Manuscript received by the Solar Energy Division, February 1988; final revision, November 1988.

The central vortex concept used in this method is based on the flow visualization study carried out in a tow tank. The experimental results are used to evaluate the empirical parameters.

Experimental Methodology

The basic blade geometry subjected to the optimization process (Fig. 1) can be defined by the following parameters:

- a blade gap size;
- b blade overlap;
- D shaft diameter;
- d rotor diameter;
- d_{disc} end plate diameter;
- H height of the wind tunnel;
- h blade height;
- $p+b$ length of the straight line portion;
- q radius of the circular arc portion;
- W width of the wind tunnel;
- θ blade circular arc angle.

To help establish the two dimensionality of the flow, end plates are used.

In general, all length parameters (except p, q) are non-dimensionalized with respect to the rotor diameter d . The non-dimensionalized blade shape parameter p/q defines the basic geometry.

Experimental approach to performance prediction requires that the model satisfy certain fluid dynamical similarity with the prototype machine. Geometric similarity is relatively easy to achieve in model fabrication. Kinematic similarity is ensured by maintaining the same tip-speed ratio for models and the prototype. Dynamic similarity is basically achieved when the operating Reynolds numbers (R_n) for the model and the full scale turbine are equal. In general, the Reynolds number has relatively small influence on the model performance. In laboratory tests, a model frequently has a smaller Reynolds number compared to the prototype. This leads the performance predicted by the model to be marginally smaller than that for a full scale machine. However, it is advisable to perform the model tests at Reynolds numbers comparable to those of the prototype turbines under field conditions.

In the present test program, relatively larger models and higher wind speeds are used to achieve comparable Reynolds numbers. This has an added advantage of better accuracy in the measurement of power and torque as well as the wind velocity.

However, the use of larger models presents the problem of wind tunnel blockage, and the associated correction could become significant. Obviously, the prediction would not be reliable unless a proper method for blockage correction is available. In this study, a set of experiments is carried out to

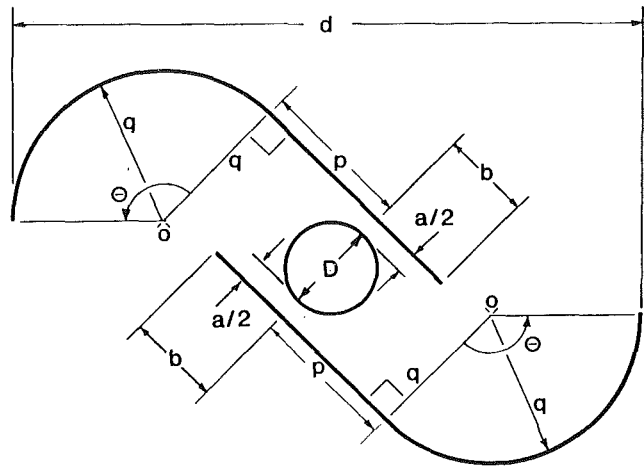


Fig. 1 Blade geometry and the associated parameters

establish the effect of blockage, thus providing an approach to obtain reliable data.

The test program involves a systematic variation of variables affecting the performance curve C_p versus λ , thus leading to an "optimum" combination of parameters.

Model tests were carried out in the boundary layer wind tunnel (Fig. 2). The partially return-type tunnel has a 2.44-m wide and 24.4-m long test section consisting of eight 3.05-m long bays. The estimated maximum turbulence level in this section is less than 0.4 percent. The tunnel can provide a stable wind speed in the range 2.5 m/s-2m/s.

The emphasis was on measurement of the torque. A hydraulic dynamometer was used for this purpose. Essentially the force was measured using a cantilever beam with four strain gauges attached near its root, two on either side. The output signal from the strain gauges, forming a part of the Wheatstone bridge, is amplified using a Bridge Amplifier Meter (BAM) and measured by a digital voltmeter. The sensitivity of the system was calculated as 0.5×10^{-3} Nm. At the beginning of each trial, the force measuring system was calibrated using known loads.

At higher rotational speeds the frictional loss due to bearings cannot be neglected. Therefore a separate set of experiments was carried out to establish the frictional power loss characteristics of the bearings.

To better understand behavior of the flow around the Savonius rotor, it was considered desirable to measure the pressure distribution along the blade. Measurements on the rotating blade are extremely difficult and need very sophisticated instrumentation. In this study, the pressure measurement is limited to the stationary blade at different angles. This provided rather important information such as

Nomenclature

a = blade gap size	F_1, F_2 = empirical parameters	Δs = length of the blade element
A = aspect ratio, h/d	h = blade height	S_1, S_2 = empirical parameters
b = blade overlap	H = height of the wind tunnel	t = time
B = blockage ratio, $(h \cdot d)/(H \cdot W)$	p, q, θ = parameters defining blade geometry	T = torque
C_p = pressure coefficient, $(p - p_\infty)/1/2\rho U^2$	p_i, p_∞ = pressure at the i^{th} tap and infinity, respectively	U = free stream velocity
C_p = power coefficient, $P/1/2\rho U^3 h d$	P = power	W = width of the tunnel
T = torque coefficient, $T/1/2\rho U^2 h d R$	(r, γ) = polar coordinates of the blade contour with respect to the main radius	β = angle of attack of the blade
d = rotor diameter	R = rotor radius, $d/2$	λ = tip-speed ratio, $d\omega/2U$
d_{disc} = end plate diameter	R_n = Reynolds number	μ = viscosity
		ν = kinematic viscosity
		ρ = density of air
		ω = angular velocity of the rotor

Axivane Series 2000 Rotor,
 2.44 m dia.,
 16 Cast aluminum blades,
 125 h.p. electric motor,
 175,000 cfm at 700 rpm,
 Fisher 480-60 pneumatic
 variable pitch control

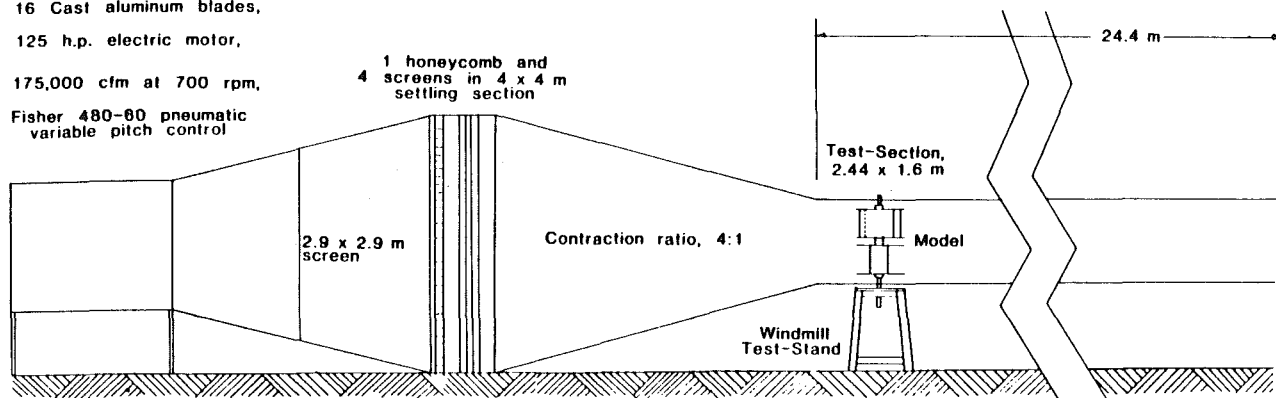


Fig. 2 Boundary layer wind tunnel used in the test program

the positions of the separation points, base pressure coefficient, etc., which proved to be useful in theoretical modeling.

The starting characteristics of the rotor is of particular interest. A set of experiments was carried out to establish the starting torque variation with the angular position.

Experimental Results

Basically two models were used in the test program. The smaller two-blade models with a projected area of 0.1 m² were primarily designed to study the effect of gap size, overlap, and aspect ratio. A high precision, straight shaft supported the blade assembly in a pair of self-aligning bearings. In this study the blade geometry parameters p/q and θ were held fixed at 1.9 and 112 deg, respectively. The model was tested in a low speed, low turbulence return-type wind tunnel with a test section of 0.91m x 0.68m (blockage 17 percent) at a wind speed of 17.9m/s. The estimated turbulence level of the tunnel is less than 0.1 percent.

Blade Gap Size, Overlap, and Aspect Ratio. The effect of percentage gap size on the maximum power coefficient is shown in Fig. 3. This clearly shows that as separation a is increased, the maximum power diminishes. The peak power coefficient of 0.158 occurred at zero gap size. By combining power coefficient versus tip-speed ratio curves for different blade overlaps, a more informative curve of maximum power coefficient versus percentage overlap was established (Fig. 4). It is apparent that an optimum value for blade overlap is around 10 percent. The plot also shows that the maximum power coefficient remains essentially unaffected for overlaps less than 10 percent.

The results showing the variation of maximum power coefficient versus aspect ratio (A) are presented in Fig. 5. The results are corrected for bearing loss. This shows an optimum aspect ratio of 0.77 giving a maximum power coefficient of 23.5 percent (at a blockage ratio of 17 percent).

Besides providing the useful information concerning the optimum blade configuration, the single-stage model study emphasized, as expected, the presence of dead spots when the blades are aligned with the wind and the rotor fails to start on its own. Thus, for self-starting of a two blade rotor, it is necessary to have at least a two-stage system with blades in the individual stage oriented orthogonal to one another. Furthermore, results suggest that to generate even 100W of power at a wind speed of 7m/s, it would require a projected area of 3.5m². In addition, the ease of fabrication being a guiding criterion, particularly in a rural environment, suggested a multistage construction. It was, therefore, decided to conduct tests with models of a two-stage rotor with a projected area of

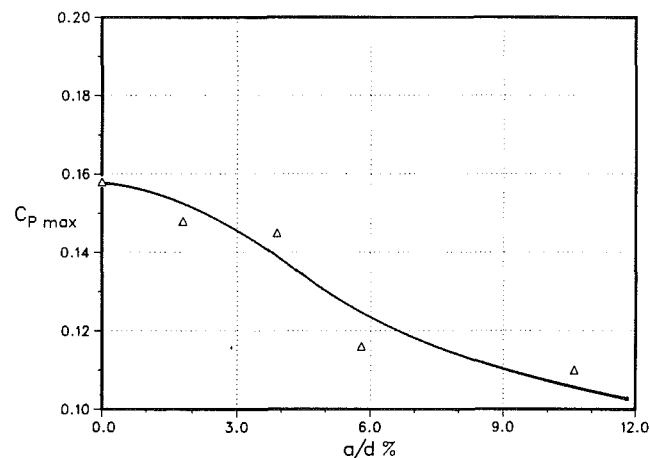


Fig. 3 Effect of gap size on peak power coefficient

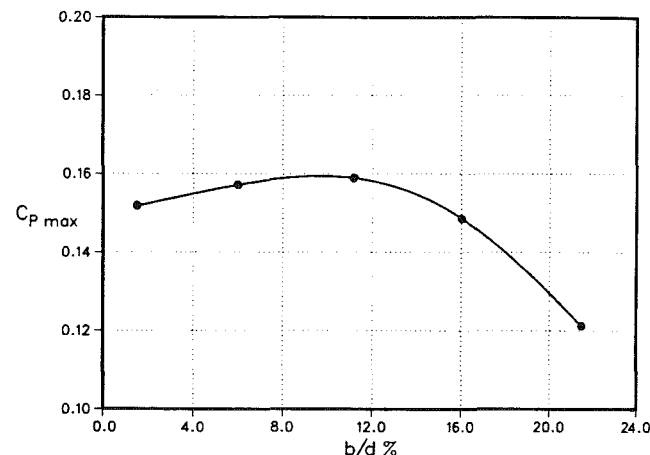


Fig. 4 Variation of the maximum power coefficient with percentage overlap

0.6m², to assess interference effects due to staging, and influence of the blade geometry parameter p/q .

Blade Shape Factors p/q and θ . It is reasonable to assume that the basic blade shape has a significant effect on its performance. As shown in Fig. 1, the parameter p/q governs the basic shape of the blade. A set of two-stage models, diameter 635mm, stage height 489mm ($A=0.77$), and end plate diameter 847mm was constructed with gauge 16 aluminum sheet to study the effect of shape factor p/q (Fig. 6). For

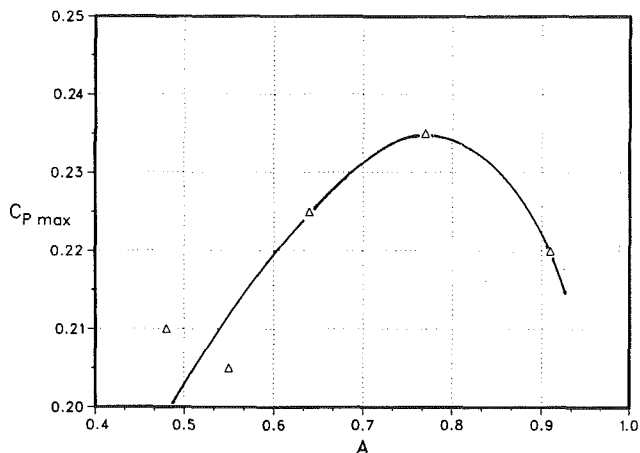


Fig. 5 Effect of blade aspect ratio on the peak power coefficient

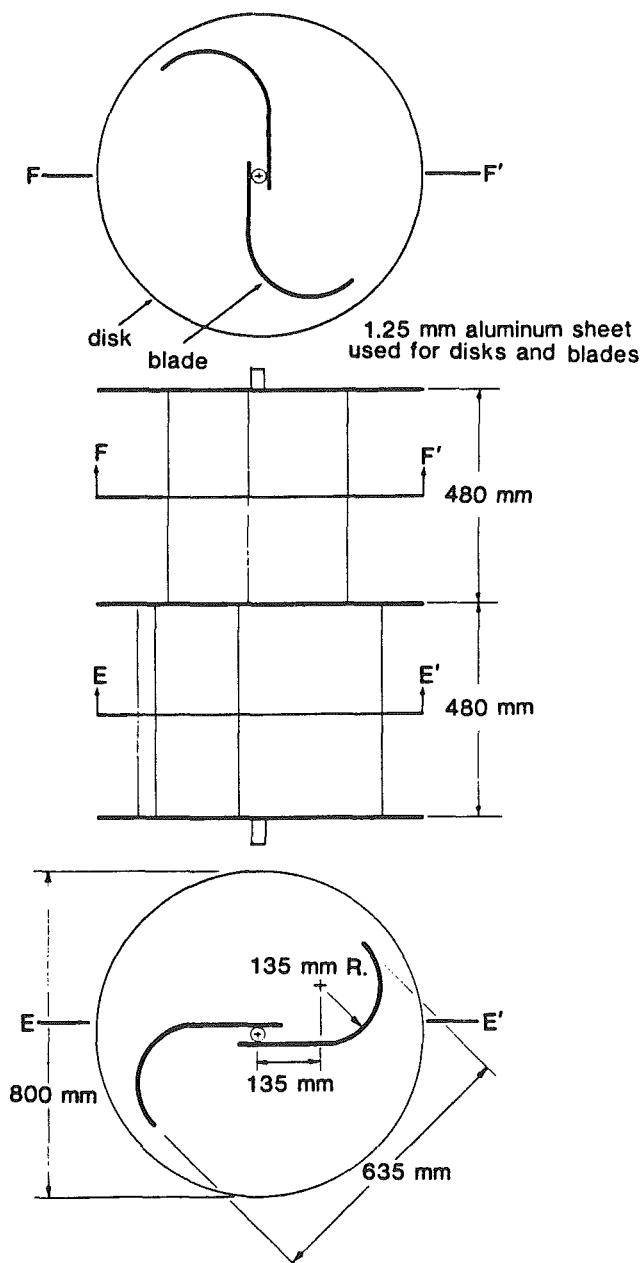


Fig. 6 A typical model of the two-stage Savonius rotor used to study the blade shape parameter p/q

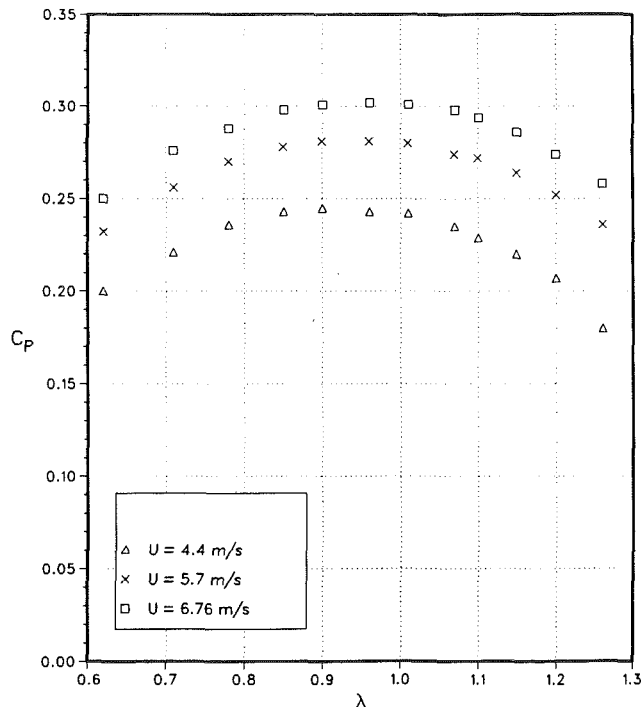


Fig. 7 Variation of power coefficient with wind speed for the two-stage rotor ($p/q = 1.6$) emphasizing the effect of bearing power loss

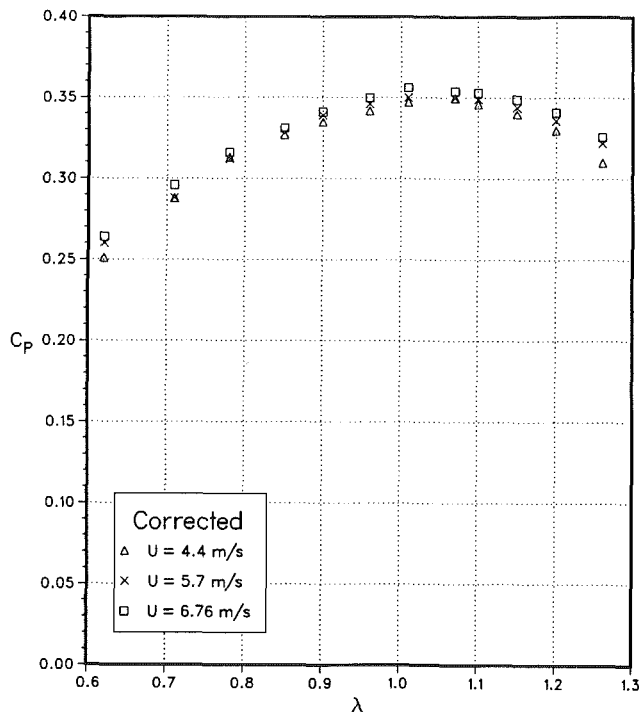


Fig. 8 Bearing loss corrected characteristic curves at three different wind speeds

simplicity in fabrication, θ was taken to be 135 deg for all models.

Uncorrected C_p versus λ curves at three different wind speeds for $p/q = 1.6$ are shown in Fig. 7. In general, one would expect variation of the power coefficient with tip-speed ratio to be essentially independent of the wind speed. However, the plots suggest a marked dependence due to the uncorrected character of the data. Accounting for the bearing, dissipation led to near collapse of the results on a single curve as shown in Fig. 8. The slight discrepancy between the corrected curves

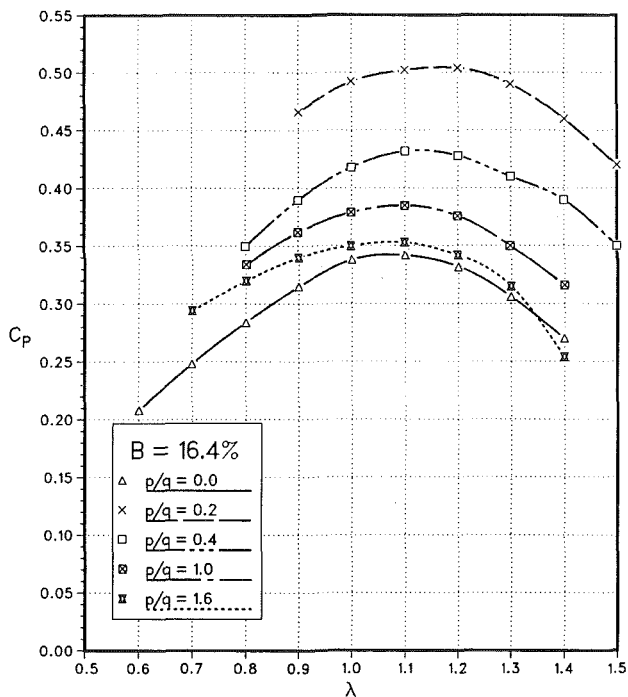


Fig. 9 Effect of p/q on the power coefficient at a constant blockage

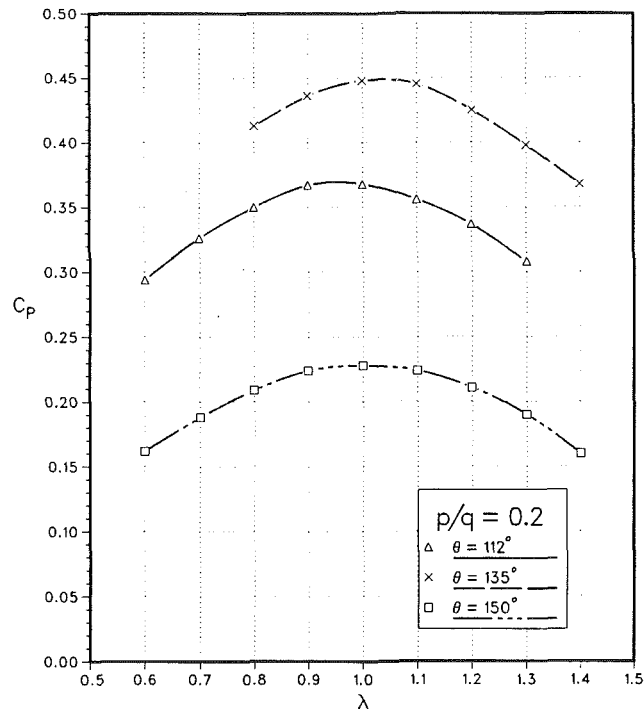


Fig. 11 Effect of the blade circular arc angle θ on the power coefficient

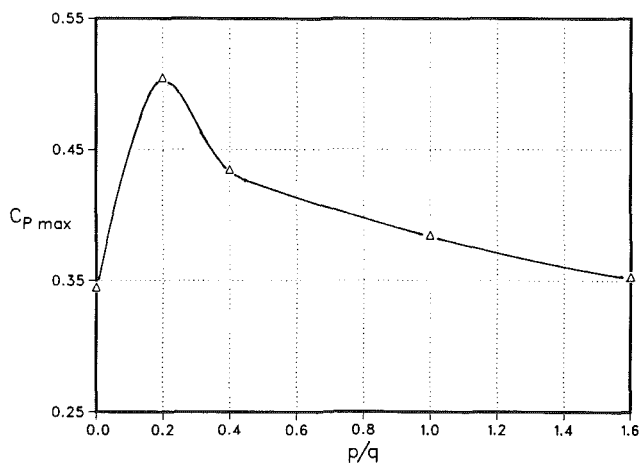


Fig. 10 Variation of the peak power coefficient with p/q at a constant blockage of 16.4 percent

may be attributed to the Reynolds number effect which, in this case, is relatively insignificant.

Corrected C_p versus λ curves for different p/q values are shown in Fig. 9. In this set of experiments the blockage ratio B was kept constant at 16.4 percent. Note, the geometric parameter p/q has a significant effect on the power coefficient. The more informative graph in Fig. 10 shows the variation of maximum power coefficient with p/q . Under the given conditions, the maximum power coefficient was found to be as high as 0.5 (uncorrected for blockage) for $p/q = 0.2$.

To investigate the effect of blade arc angle, a set of single-stage rotors with $p/q = 0.2$ and 10 percent blockage were constructed. Their projected area was $\approx 0.37\text{m}^2$. The corrected C_p versus λ curves for $\theta = 112, 135,$ and 150 degs, presented in Fig. 11, suggest the optimum value for θ to be around 135 deg.

The operating Reynolds number of the prototype turbine would be around $3 \times 10^5 - 9 \times 10^5$. On the other hand, most of the wind tunnel tests were carried out in the Reynolds number range $1.7 \times 10^5 - 4 \times 10^5$. Fortunately, C_p versus λ plots (not shown) suggested that the effect of the Reynolds number in the operating range is likely to be insignificant.

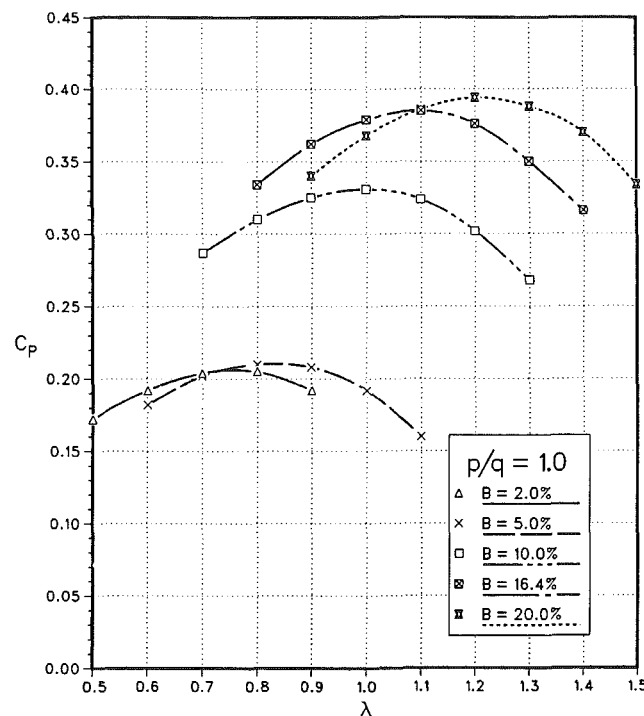


Fig. 12 Effect of blockage on power output of the Savonius rotor

Blockage Ratio. Wind tunnel results presented by different investigators often do not correlate because of different test conditions. One of the major parameters affecting the test data is the blockage.

To have some appreciation of the wall confinement effects, models with an identical geometric shape, but with different blockage ratios, were tested in the boundary layer wind tunnel. The results presented in Fig. 12 clearly show a dramatic increase in the maximum power coefficient, primarily due to an increase in the local velocity, with blockage. Note that an increase in wall confinement from 5 to 20 percent can raise the $C_{p_{max}}$ by around 70 percent, thus leading to a highly optimistic

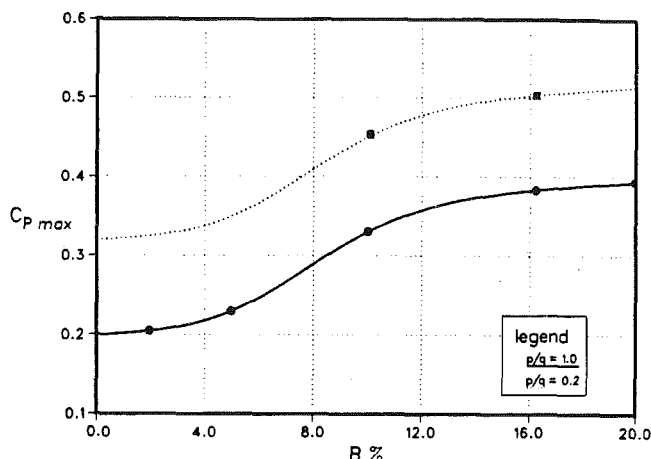


Fig. 13(a) Effect of blockage on peak power coefficient for two different blade geometries

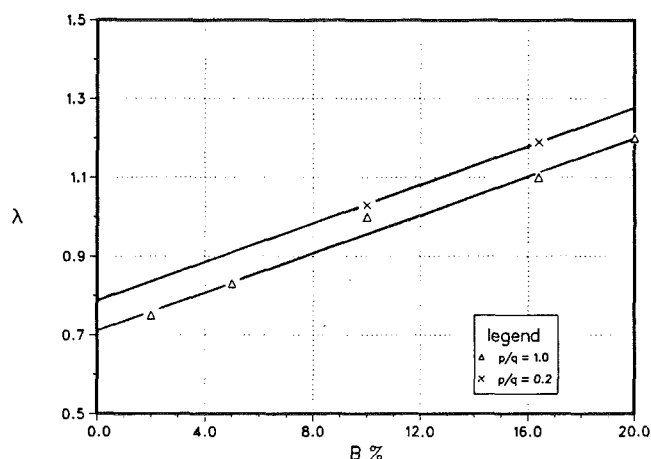


Fig. 13(b) Effect of blockage on the tip speed ratio at peak power coefficient for two blade geometries

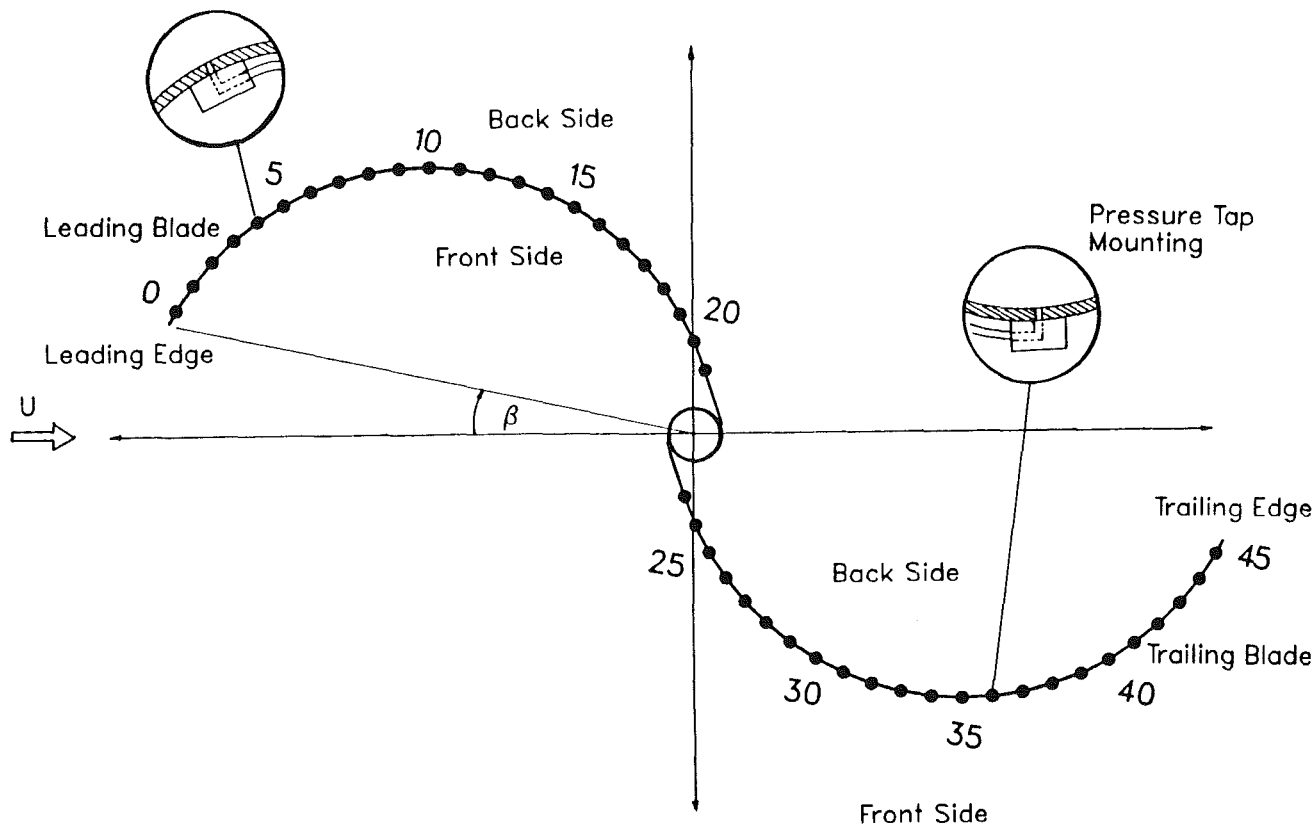


Fig. 14 Pressure tap location and numbering scheme

performance if the blockage effect is not corrected.

Figure 13(a) shows the variation of $C_{p\max}$ with blockage B for $p/q = 1$. It should also be noted that when operating in the unconfined environment, the power coefficient reduces to 0.2. To obtain similar information at other p/q values would involve an extensive test program. However, of particular interest here is the corrected power coefficient corresponding to the optimum p/q of 0.2. To this end, two models with blockage ratios of 10 percent and 16.4 percent were constructed. Recognizing the fact that the associated wake aerodynamics remains essentially the same, the variation of $C_{p\max}$ with blockage is expected to have the same trend. This suggests that the Savonius rotor with an optimum combination of parameters has an efficiency of about 32 percent in unconfined conditions.

The plot of tip-speed ratio (λ) at the peak power coefficient versus B (Fig. 13(b)) shows a linear variation. This yields the

zero blockage values of λ as 0.71 and 0.79 for $p/q = 1.0$ and 0.2, respectively.

The systematic optimization process has indeed proved to be quite rewarding. By conducting a series of carefully planned experiments, it has been possible to improve the rotor performance by a factor of two.

The optimum blade configuration (for the end plate parameter $d/d_{\text{disc}} = 0.75$) can be summarized as follows:

a/d	nondimensional blade gap size	= 0;
b/d	nondimensional blade overlap	= 0;
A	blade aspect ratio	= 0.77;
p/q	blade shape parameter	= 0.2;
θ	blade arc angle	= 135 deg.

Pressure Distribution. An extensive test program aimed at determining the pressure distribution on the surface of the rotor blades was undertaken using a single-stage Savonius

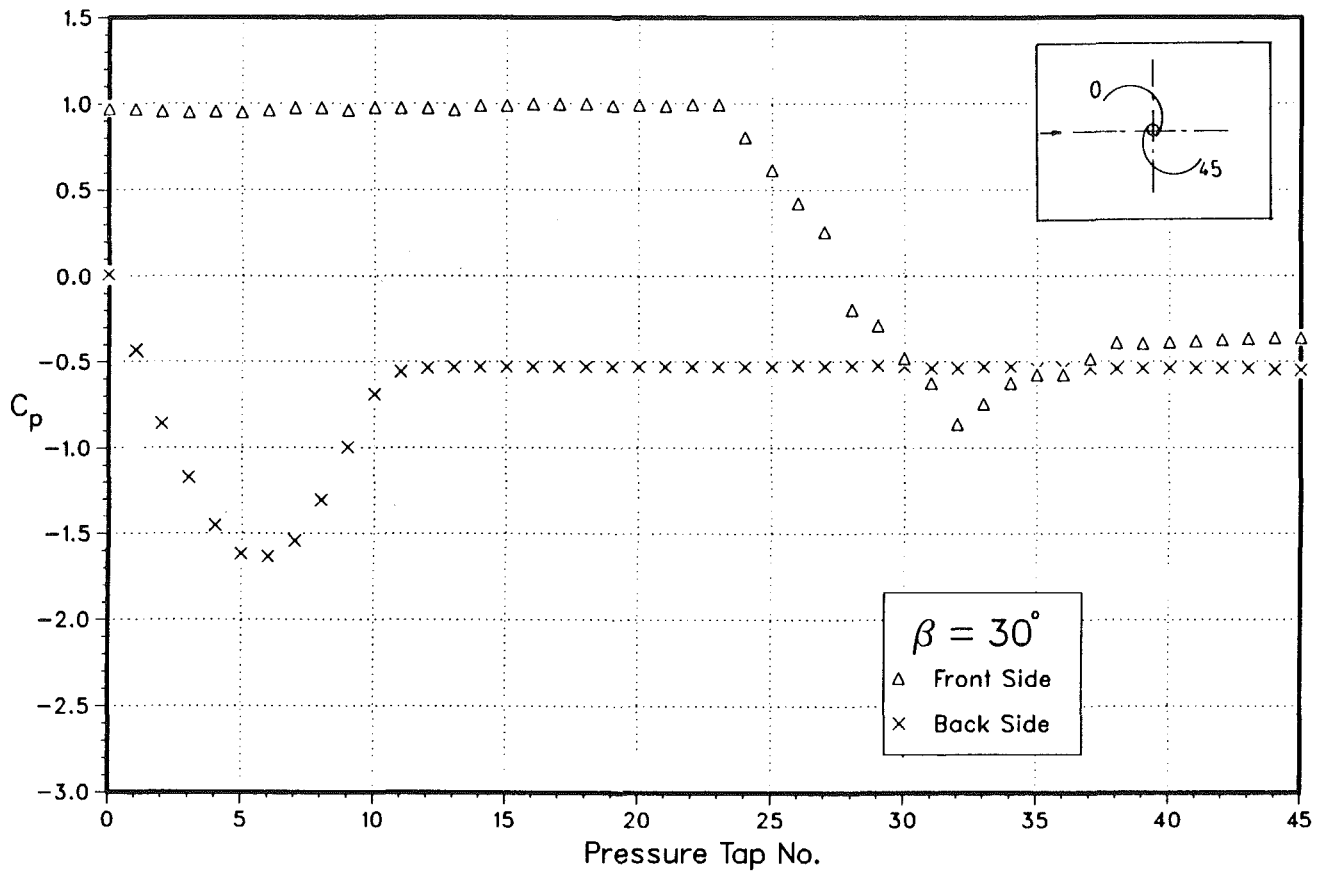


Fig. 15(a) Surface pressure distribution over the Savonius blade at $\beta = 30$ deg

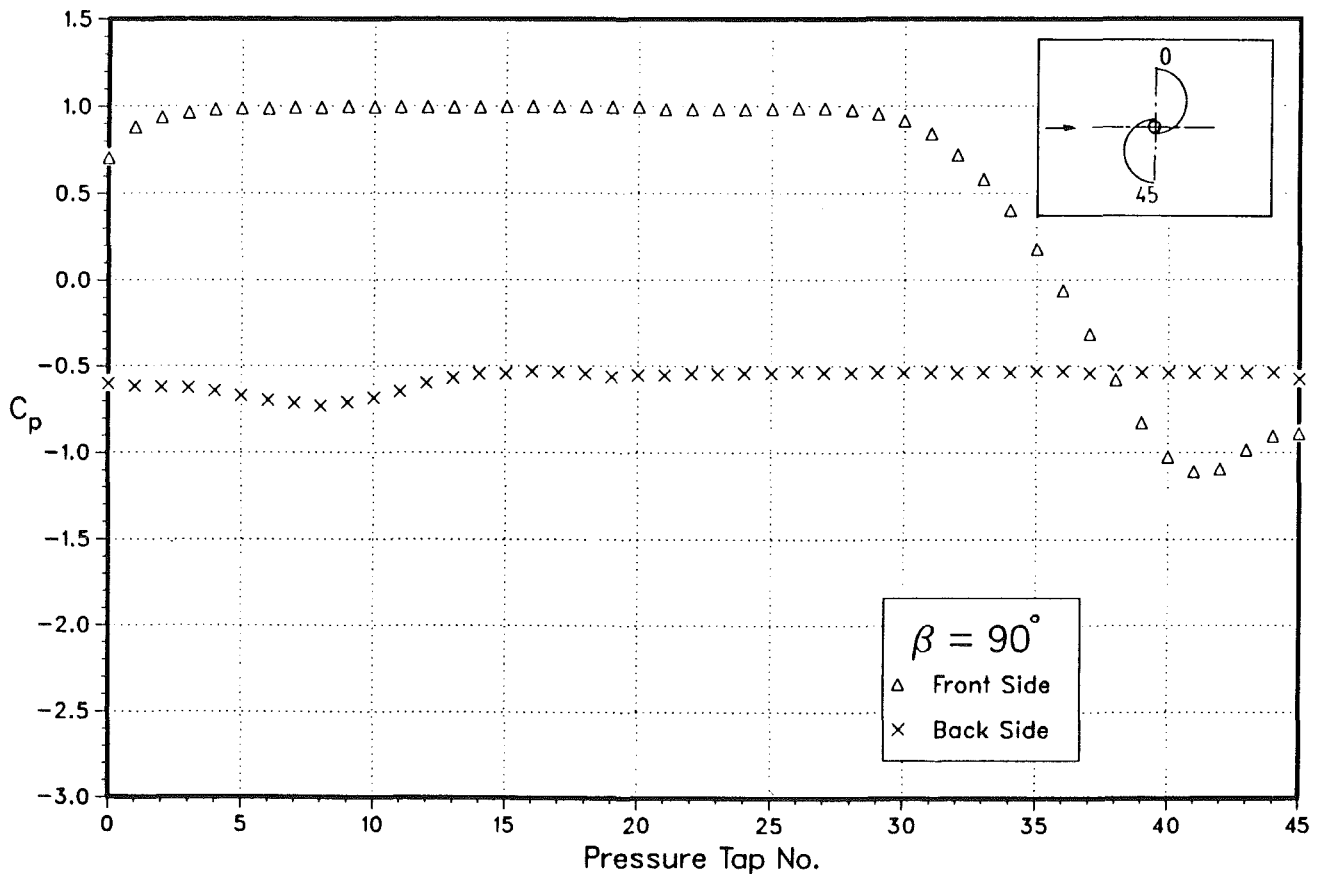


Fig. 15(b) Surface pressure distribution over the Savonius blade at $\beta = 90$ deg

rotor with optimum geometric parameters and 10 percent blockage. The blades were provided with 46 pressure taps distributed as indicated in Fig. 14. The amount of information obtained is rather enormous, however, only a typical set of results useful in establishing trends is presented here.

Obviously the local flow is rather complex with cause and effects often eluding detection. At $\beta=30$ deg (Fig. 15(a)), pressure on the front side remains at the stagnation value for the leading blade followed by a sharp drop. The reverse curvature causes an adverse pressure gradient and the flow separates around the 38th tap. The pressure on the back side decreases when the flow accelerates along the convex surface of the leading blade, goes through the familiar variation and separates at the 11th tap. Thus there are two separation points, one on the back side of the leading blade and the other on the front side of the trailing blade.

Separation points move to the tips at $\beta=90$ deg (Fig. 15(b)) as characterized by the constant back pressure. The smooth pressure drop along the front side of the trailing blade suggests accelerating flow and is followed by a partial pressure recovery before separation at the trailing edge. Similar pressure variations were observed for β up to 140 deg.

Starting Torque. The starting torque coefficient for the 10 percent blockage model with optimum blade geometry was measured at two wind speeds and is shown in Fig. 16. Note, the effect of Reynolds number is minimal substantiating the earlier observations. The line represents the torque calculated through pressure integration assuming two dimensionality. The deviation between measured and calculated values is within an acceptable error margin (maximum error ≈ 5 percent). This suggests that the assumption of two dimensional flow is reasonable for this class of models.

Fig. 16 shows a positive torque over the range of $\beta \approx 0$

deg – 130 followed by the torque reversal. The peak positive torque occurs at around 30 deg suggesting that this rotor is not exactly a drag device.

Semi-Empirical Approach

Inadequacy of the Quasi-Steady Approach. Consider the classical quasi-steady approach, which has been successfully applied in the analysis of the Darrieus rotor as well as various other fluid dynamics problems. Here the blade is divided into a finite number of elements assuming two-dimensional flow. For a given angular position of the blade, contributions of the free stream velocity and the blade rotation at each element is determined using velocity triangles (Fig. 17). Here, (r_i, γ_i) are the polar coordinates at the center of the i^{th} element with respect to the diameter of the rotor. Ψ_i is the angle between the normal vector and the radius vector. β_i is the blade angle with respect to the relative velocity V_i at the i^{th} element, and ω is the angular velocity of the turbine. The mean differential pressure coefficient obtained experimentally, at the i^{th} element for the blade angle $\beta = \beta_i$ was used in conjunction with the relative velocity V_i to evaluate the force acting on this element. In the present study, pressure distribution was measured at ten intervals. Linear interpolation was used to estimate the pressure coefficients at intermediate locations. Using an appropriate moment arm for the blade element, integration over the blade gave the torque for a specified position β of the rotor. Finally, by evaluating the work done over a cycle, the mean power and power coefficient were established. Repeated the procedure for different angular velocities the effect of tip-speed ratio on the power coefficient was estimated.

The results obtained using this procedure are compared with the corresponding experimental results (for $p/q=0.2$, $B=10$ percent, $\theta=135$ deg model) in Fig. 18. The large discrepancy between results suggests that the classical quasi-steady ap-

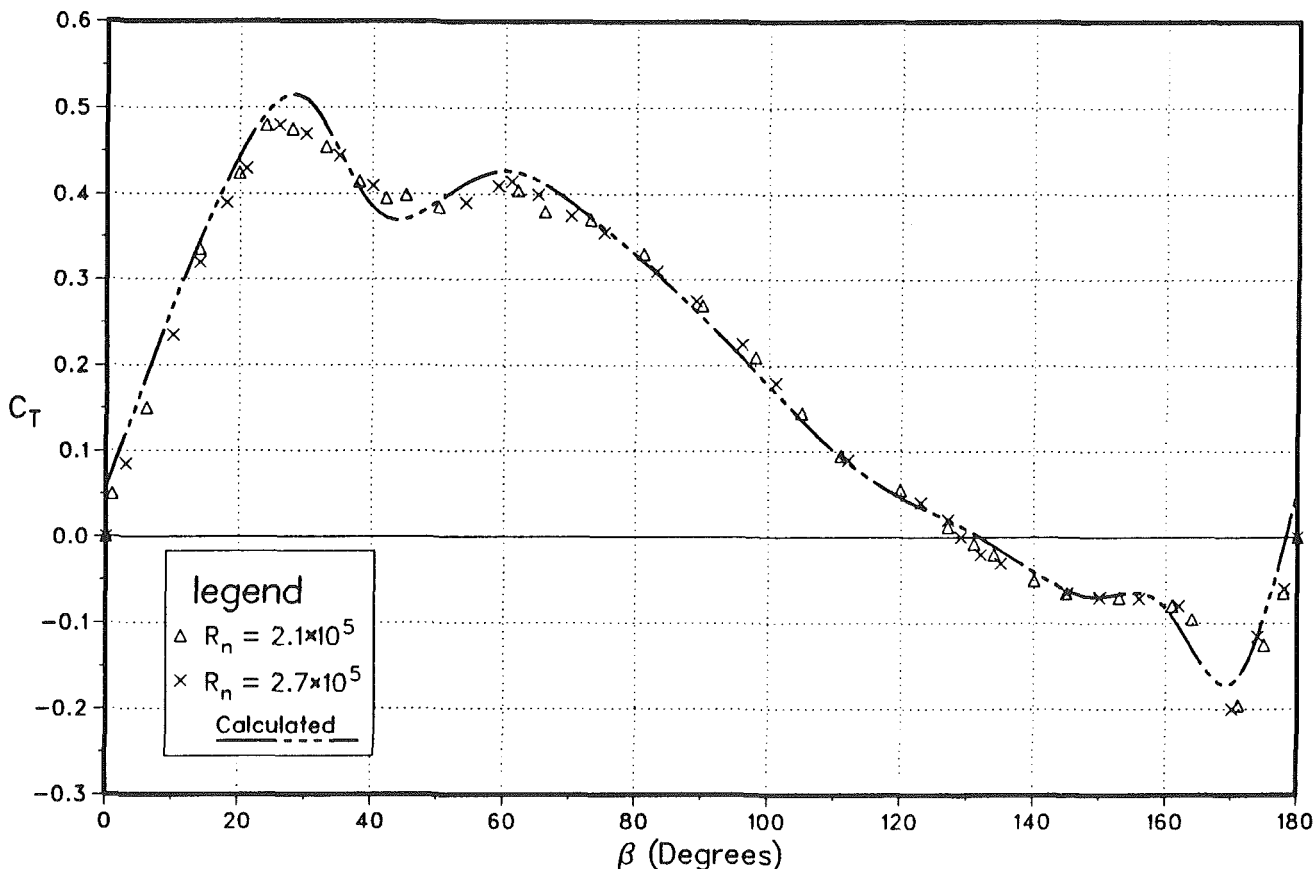


Fig. 16 Variation of the starting torque with angular position of the Savonius rotor ($p/q = 0.2$, $B = 10$ percent)

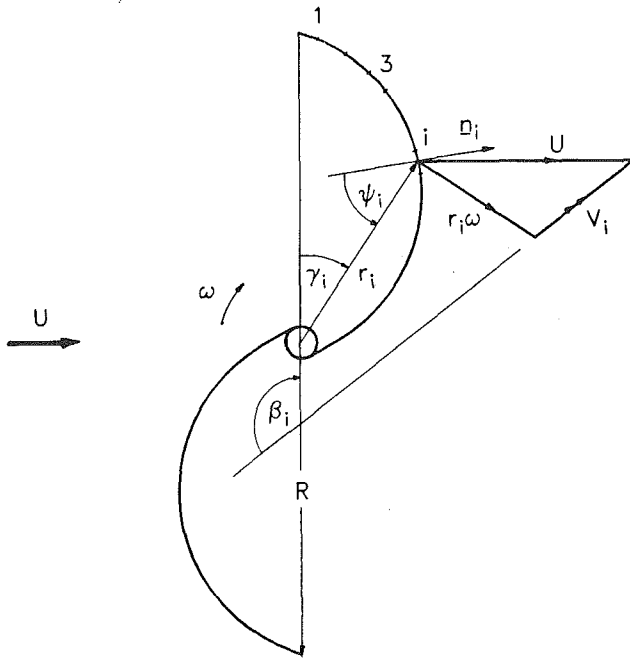


Fig. 17 A typical velocity triangle at the blade element i combining the effect of free stream velocity and blade rotation

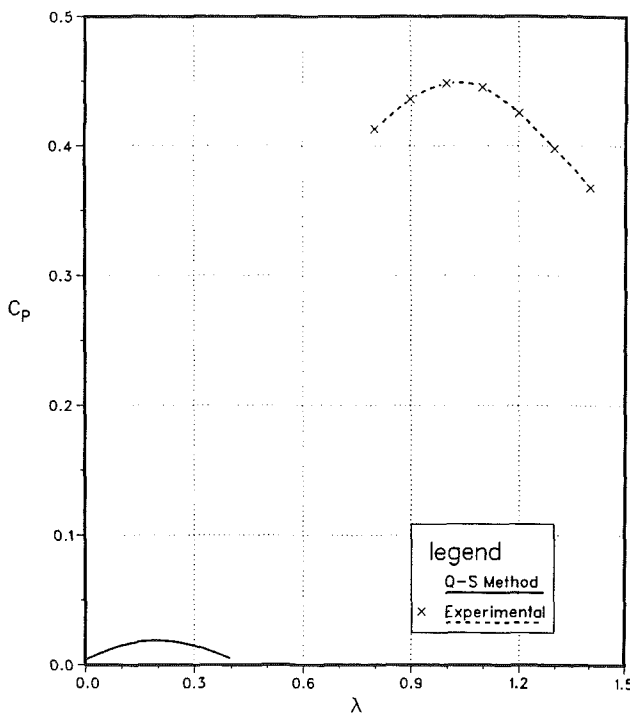


Fig. 18 Results of the quasi-steady analysis

proach is not successful in predicting the Savonius rotor performance. This may be attributed to disparity in the flow features associated with the stationary and rotational modes of the blade. The method, however, proved effective with the Darrieus rotor, where the flow character does show a degree of similarity. In the present case, since the relative direction of the flow varies significantly along the blade, interactions between elements of the rotor cannot be neglected. Unfortunately, the classical quasi-steady approach does not account for these interactions. Thus, this approach cannot be used effectively to analyze the Savonius rotor.

Modified Quasi-Steady Approach. Failure of the classical

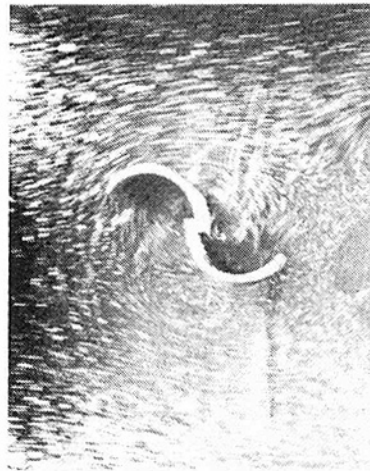
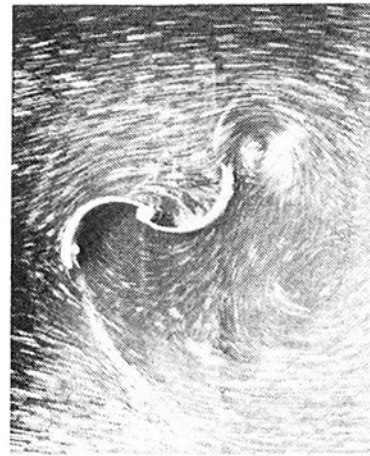


Fig. 19 A typical set of flow visualization pictures showing the presence of the central vortex filament

quasi-steady procedure emphasized the need for an alternative. It was apparent that clear understanding of the flow character was a prerequisite to approach the problem. To better appreciate the basic character of the flow around the Savonius rotor, a flow visualization study was undertaken.

A typical set of pictures obtained are shown in Fig. 19. Perhaps the most significant feature is the central vortex filament in the time-averaged flow. The existence of this vortex has also been reported in literature [2].

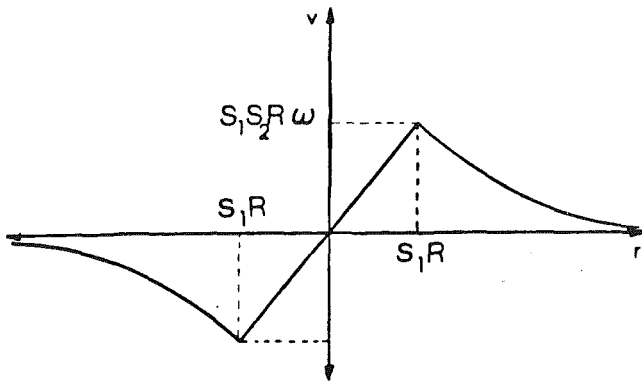


Fig. 20 Velocity distribution due to the central vortex

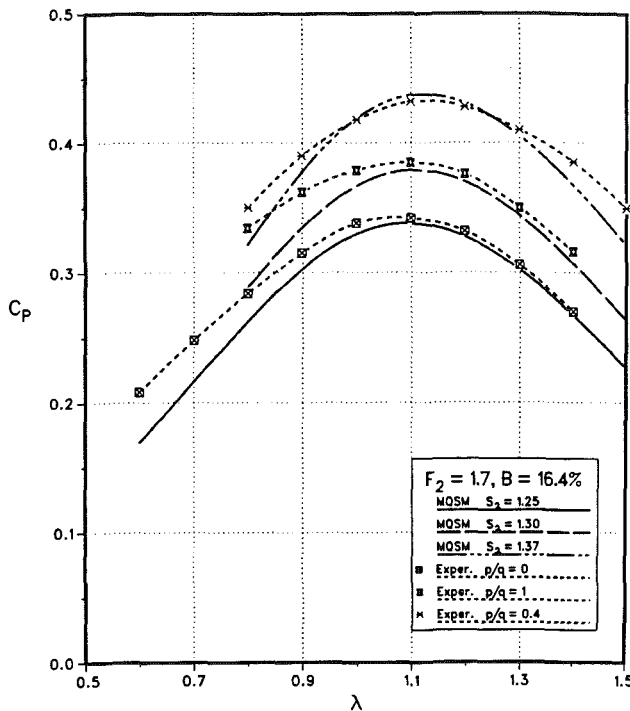


Fig. 21 Identification of the parameter S_2 as a function of p/q when F_2 and blockage are kept constant

The flow visualization study provided a rational modification of the classical quasi-steady approach to the problem by introduction of a central vortex filament. The flow is simulated by a potential vortex with a core radius S_1R , a core angular velocity $S_2\omega$, and a uniform free-stream velocity U . Here R and ω represent radius and angular speed of the rotor, respectively, and S_1, S_2 are two empirical parameters. The velocity distribution of the vortex filament is shown in Fig. 20.

The relative velocity at each element is evaluated using the modified flow field and the angular speed of the rotor. Force at the individual element is evaluated using the differential pressure coefficient and the velocity of the resultant flow as discussed earlier. The procedure leads to evaluation of power coefficient C_p in terms of tip-speed ratio λ, S_1 , and S_2 .

S_1 and S_2 were systematically varied and the corresponding C_p estimated over a range of tip-speed ratio $\lambda = 0.6 - 1.5$. The results obtained, when compared to the experimental results, suggested the functional relations:

$$C_p = C_p(S_1, S_2); \quad (1)$$

$$S_1 = F_1(\lambda) + F_2(B, R_n); \quad (2)$$

$$S_2 = S_2(p/q, R_n); \quad (3)$$

as logical. The effect of tip-speed ratio could be absorbed in

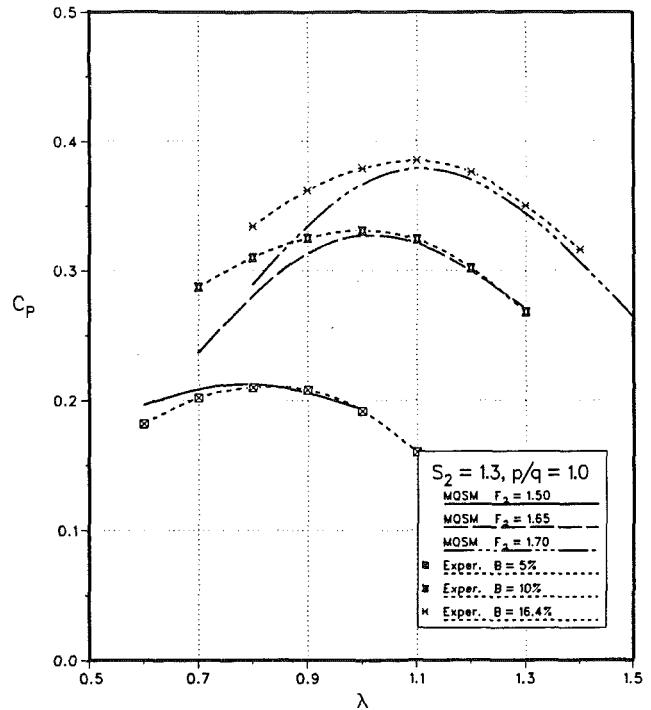


Fig. 22 Identification of the parameter F_2 as a function of blockage when S_2 and p/q are kept constant

S_1 , while S_2 showed a direct dependence on the variation of the geometric parameter p/q . The remainder of S_1 , when varied, appeared to model the blockage effect. Influence of the Reynolds number (R_n) is included here in both S_1 and S_2 , however, as seen before, it is insignificant in the operating range. Using the experimental results for $p/q = 0, B = 16.4$ percent, $F_1(\lambda)$ can be expressed as,

$$F_1(\lambda) = 0.27778\lambda^2 - 1.08333\lambda, \quad (4)$$

with corresponding values for F_2 and S_2 as 1.7 and 1.25, respectively. According to the suggested functional forms, $F_2 = 1.7$ combined with different S_2 should produce a set of results corresponding to performance of constant blockage (16.4 percent) models with different p/q values. As shown in Fig. 21, the calculated results for $S_2 = 1.25, 1.3, 1.37$, agree with experimental curves of $p/q = 0, 1.0, 0.4$ at $B = 16.4$ percent, respectively, when F_2 is kept constant at 1.7. Similarly, when S_2 is kept constant at 1.3 (corresponding to $p/q = 1$) and F_2 is varied, this should simulate results for $p/q = 1$ models with different blockage ratios. The results shown in Fig. 22 verifies this prediction. Now it is evident that the aforementioned functional forms can be used to predict the performance of Savonius rotors, if the relationship between F_2 and blockage ratio, and S_2 and p/q can be established for the operating R_n range.

The agreement between calculated and experimental results shown in Fig. 21 and Fig. 22 is used to establish S_2 and F_2 in terms of p/q and B , respectively. The empirical curves established for S_2 and F_2 for the operating Reynolds number range are shown in Fig. 23.

Results and General Remarks. C_p versus λ curve for $p/q = 0.2$ and $p/q = 1.6$ at $B = 16.4$ percent were obtained experimentally and were not used to establish the empirical relations in the modified quasi-steady approach. Similarly, the experimental results for $p/q = 0.2, B = 10$ percent were not involved in the development of the method. Therefore, these three cases can be used to verify the validity of the previously stated approach. The comparison of the predictions given by the modified quasi-steady approach with the experimental results for these three cases are shown in Fig. 24.

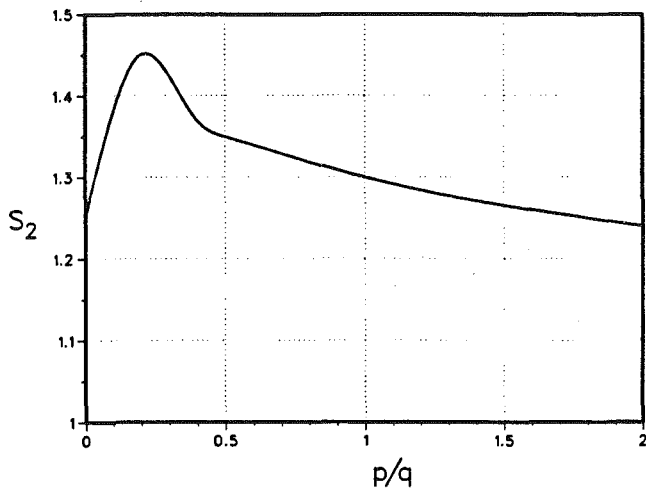


Fig. 23(a) Empirical relationship between S_2 and p/q

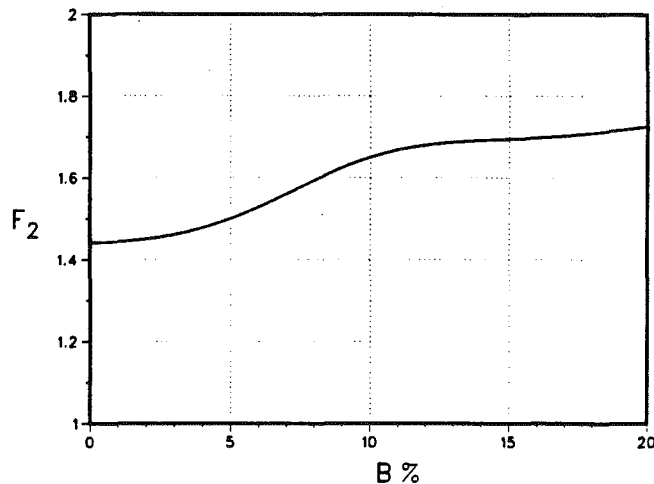


Fig. 23(b) Empirical relationship between F_2 and B

From engineering design considerations, the agreement may be considered quite acceptable although the results are under-predicted at lower tip-speed ratios.

Superposition of the central vortex filament assumes a potential flow field. But the time-dependent shear layers, separated flow, and high turbulence levels suggest that the flow field is far from being potential. Furthermore, the wake is not considered in this analysis. However, within its limitations, the method permits prediction of model performance in the wind tunnel, as well as that of the prototype, with a reasonable accuracy.

Concluding Remarks

Based on the wind tunnel test program, flow visualization study, and semiempirical modeling of the Savonius rotor, the following general conclusions can be made:

(a) The optimum configuration of the Savonius rotor corresponds to the blade geometry as follows:

- gap size (a/d) = 0;
- blade overlap (b/d) = 0;
- aspect ratio (A) = 0.77;
- blade shape parameters (p/q) = 0.2;
- blade arc angle (θ) = 135 deg.

It is inferred that this has a peak power coefficient of around 0.32 at a tip-speed ratio of 0.79 (with a possible error of $\pm 5-10$ percent) in the unconfined condition representing a twofold improvement in performance compared to the reported values in literature ($\approx 0.12-0.15$). This brings it

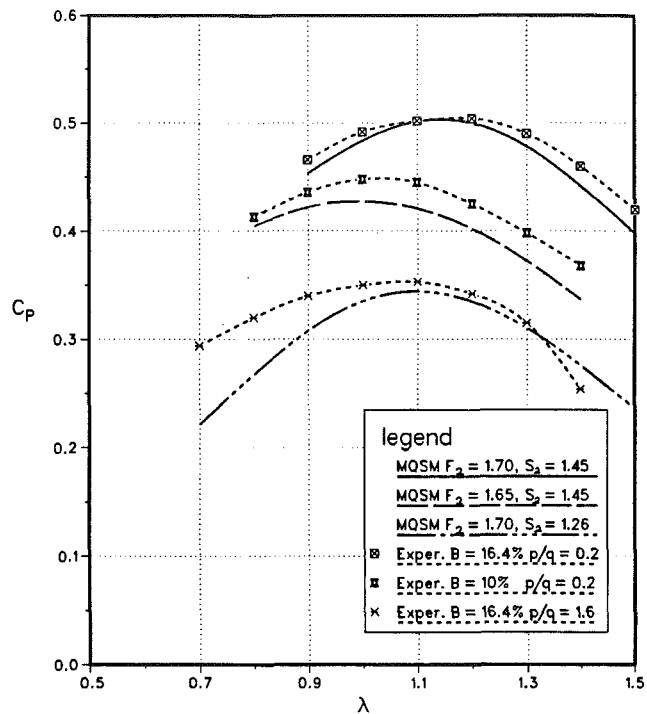


Fig. 24 Predictions of the modified quasi-steady approach compared to the experimental results

close to more sophisticated and costly configurations like the Darrieus design in terms of performance, yet retaining its simplicity and self-starting character.

(b) Characteristic plots of C_p versus λ suggest that the Savonius rotor is not a pure drag device. This is logical as at small β the rotor behaves like a slender body with lift contributing to the power.

(c) The effect of blockage is to increase the peak power coefficient and the corresponding tip-speed ratio. A variation in the blade shape parameter (p/q) shifts the $C_{p, \max}$ versus blockage plot along the ordinate without affecting its general shape.

(d) The semi-empirical approach using experimentally established parameters can predict performance of the rotor with a reasonable accuracy.

(e) Presence of a vortex filament at the center of the rotor is also confirmed through the flow visualization study.

References

- 1 Templin, R. J., and South, P., "Some Design Aspects of High Speed Vertical Axis Wind Turbines," *Proceedings of the First International Symposium on Wind Energy Systems*, BHRA, Cambridge, U. K., Sept. 1976.
- 2 Jones, C. N., Litter, R. D., and Manser, B. L., "The Savonius Rotor-Performance and Flow," *Proceedings of the First BWEA Wind Energy Workshop*, 1979, pp. 102-108.
- 3 Savonius, S. J., "The S-Rotor and its Application," *Mechanical Engineering*, Vol. 53, No. 5, 1931, pp. 333-338.
- 4 Shankar, P. N., "The Effects of Geometry and Reynolds Number on Savonius Type Rotors," Technical Memorandum, AE-TM-3-76, National Aeronautical Laboratory, Bangalore, 1976.
- 5 Sivasegaram, S., "Design Parameters Affecting the Performance of the Resistant Type Vertical Axis Wind Rotors," *Wind Engineering*, Vol. 1, No. 3, 1977, pp. 207-217.
- 6 Sivasegaram, S., "Concentration Augmentation of Power in a Savonius Type Wind Rotor," *Wind Engineering*, Vol. 3, No. 1, 1979, pp. 52-61.
- 7 Bach, Von G., "Untersuchungen Über Savonius Rotoren und Verwandte Stromungsmaschinen," *Forsh. auf dem Gebiete des Ingenieurwesens*, Vol. 2, 1931, pp. 218-231 (in German).
- 8 Newman, B. G., "Measurements on Savonius Rotor with Variable Gap," *Proceedings of the Sherbrooke University Symposium on Wind Energy*, Sherbrooke, Canada, 1974, p. 116.
- 9 Khan, M. H., "Model and Prototype Performance Characteristics of the Savonius Rotor Windmill," *Wind Engineering*, Vol. 2, No. 2, 1978, pp. 75-85.
- 10 Blackwell, B. F., and Feltz, L. V., "Wind Energy a Revitalized Pursuit," Report SAND-75-01666, Sandia Laboratories, Albuquerque, N. Mex., 1975.